

Global sensitivity analysis in the limited data setting with application to char combustion

Dongjin Lee^{a,*}, Elle Lavichant^a, Boris Kramer^{a,*}

^a*Department of Mechanical and Aerospace Engineering, University of California San Diego, CA, United States*

July 17, 2023

Abstract

In uncertainty quantification, variance-based global sensitivity analysis quantitatively determines the effect of each input random variable on the output by partitioning the total output variance into contributions from each input. However, computing conditional expectations can be prohibitively costly when working with expensive-to-evaluate models. Surrogate models can accelerate this, yet their accuracy depends on the quality and quantity of training data, which is expensive to generate (experimentally or computationally) for complex engineering systems. Thus, methods that work with limited data are desirable. We propose a diffeomorphic modulation under observable response preserving homotopy (D-MORPH) regression to train a polynomial dimensional decomposition surrogate of the output that minimizes the number of training data. The new method first computes a sparse Lasso solution and uses it to define the cost function. A subsequent D-MORPH regression minimizes the difference between the D-MORPH and Lasso solution. The resulting D-MORPH surrogate is more robust to input variations and more accurate with limited training data. We illustrate the accuracy and computational efficiency of the new surrogate for global sensitivity analysis using mathematical functions and an expensive-to-simulate model of char combustion. The new method is highly efficient, requiring only 15% of the training data compared to conventional regression.

Keywords: Global sensitivity analysis, ANOVA, polynomial dimensional decomposition, surrogate modeling, D-MORPH regression, char combustion

1. Introduction

Global sensitivity analysis is a powerful tool in uncertainty quantification to measure the influence of input variables on the quantity of interest (QoI), or output, of a simulation model. Global sensitivity analysis helped scientists and engineers identify the most influential input variables and to make better decisions concerning system design and operation in a broad range of applications, including space weather [9, 8], biological systems [11, 18], structural engineering [10, 26], or wind energy [1]. In contrast to local sensitivity analysis that determines the gradients of the output with respect to variations in each input, the global sensitivity analysis explores the full range of the input variables, providing a more complete picture [22, 25]. Consider, for instance, an engineering system (e.g., a power plant) with three operating or design inputs that are mapped via a simulation to a QoI. When implementing quantitative global sensitivity analysis, one may find that one input possesses a sensitivity of 90% to the QoI, whereas the combined sensitivity index of the other two inputs contributes only 10% to the variation of the QoI. Methods to optimize the system or quantify its uncertainty, often scale badly with the number of input variables due to the curse of dimensionality [14, 12]. Global sensitivity analysis can assist the system designer by providing quantitative reasons to neglect the two parameters that only contribute 10% to variations in the QoI and focusing only on the most influential parameter.

*Corresponding author

Email addresses: dongjin-lee@ucsd.edu (Dongjin Lee), bmramer@ucsd.edu (Boris Kramer)

Variance-based sensitivity analysis (also called ANalysis Of VAriance (ANOVA) or Sobol sensitivity analysis [28]) is a popular class of global sensitivity analysis methods that estimates the sensitivity of the QoI to each input variable by partitioning the total variance of the output into contributions from each input variable [22]. Variance-based methods are formulated as conditional variances and can be evaluated by Monte Carlo simulation or Latin hypercube sampling [6], see also the review [29]. These sampling methods often face difficulties when applied to a computationally intensive model. Numerous global sensitivity analysis studies therefore leverage efficient surrogate models, such as polynomial chaos expansion (PCE) [29], polynomial dimensional decomposition (PDD) [25], reduced-order modeling [23], Gaussian process or Kriging [30], support vector machine [2], and artificial neural network [17]. The authors in [23] present a multifidelity framework for global sensitivity analysis that combines a high-fidelity model with multiple low-fidelity models to efficiently provide unbiased estimates of global sensitivity measures. Among these surrogate models, PDD, which is a Fourier-polynomial expansion of lower-variate component functions [24], is one of the most effective surrogates for global sensitivity analysis. The PDD surrogate truncates its bases effectively in a dimension-wise manner which, to some effect, alleviates the curse of dimensionality compared to PCE. The PDD surrogate, similar to ANOVA, partitions the variance of a QoI among its different input variables, enabling variance-based sensitivity analysis [25]. The accuracy of PDD depends on the number of training samples. When using conventional regression methods (e.g., standard least squares) to compute the surrogate, the number of training samples must exceed the number of to-be-learned expansion coefficients. Otherwise, we need to reduce the number of PDD bases, which degrades its accuracy relative to the QoI. As is often the case for nonlinear QoIs, the PDD surrogate can require several hundreds to thousands of training samples. Given that each training sample is obtained via an expensive simulation (e.g., in our application of char combustion in Section 5, one simulation takes 7.9 CPU hours) training the PDD model becomes impractical. Instead of reducing the basis size, one can solve an underdetermined linear system to train the surrogate model. The authors in [15, 16] introduce the diffeomorphic modulation under observable response preserving homotopy (D-MORPH) regression. The D-MORPH regression finds a solution to the linear system, and hence a surrogate model, that exactly fits the training data and minimizes the variance of the surrogate predictions [15]. When minimizing the cost function, D-MORPH assigns weights to the unknown regression solution. The resulting D-MORPH-based solution is highly sensitive to this weight selection. Although the authors in [15, 16] provide strategies for selecting these weights, their methods are specific to a particular problem and require generalization to be applicable across different problems. In [13], the authors use a D-MORPH regression to train the generalized polynomial chaos expansion surrogate for dependent inputs. The D-MORPH method partitions the surrogate basis functions into two groups. The first group consists of fewer lower-order basis functions than the number of training samples, which ensures the accuracy of the solution. The second group consists of the higher-order basis functions, which are assumed to have expansion coefficients with smaller magnitude compared to those in the primary group. However, this assumption may not hold in practical problems, requiring a more general version of the D-MORPH regression. In [5] a least absolute shrinkage and selection operator (Lasso) regression is used to train a PDD surrogate. The Lasso regression includes a regularization term that penalizes the L1 norm of the regression coefficients. While the Lasso regression effectively yields sparse solutions for underdetermined systems, it induces a bias into the QoI estimates in an effort to decrease the variance. Moreover, the Lasso regression can only infer as many non-zero coefficients as there are training samples.

In this work, we develop a new regression method to compute PDD surrogate in the limited data setting, where the linear systems for the surrogate coefficients are underdetermined. In the new method, we first compute a sparse—yet biased—Lasso solution to the underdetermined system for the PDD coefficients. We then define a new cost function that represents the difference between the D-MORPH and the Lasso-based estimates. The D-MORPH framework minimizes this cost function iteratively while maintaining the training data fit. In leveraging both the D-MORPH and Lasso regression, we obtain a surrogate that is more robust to variations in inputs and produces more

accurate solutions with limited training samples. We demonstrate the accuracy and the computational efficiency of the new regression method for global sensitivity analysis using mathematical functions. We evaluate the new regression method for an expensive-to-simulate char combustion simulation model. This simulation is based on the Eulerian framework for gas behavior and the Lagrangian framework for solid particle behavior and includes chemical kinetics models. A single simulation requires 7.9 CPU hours in a parallelized implementation with 15 CPUs. Through the new method, we reduce the necessary training samples to only 15% of the data required for a conventional regression.

The paper is organized as follows. Section 2 covers the theoretical background, the problem setting, and briefly introduces global sensitivity analysis, the PDD surrogate, and the original D-MORPH regression. Section 3 proposes a novel D-MORPH regression to train the PDD surrogate. Therein, we demonstrate the proposed method using two mathematical functions. Section 4 uses the proposed method for global sensitivity analysis of char combustion, where we only need 151 samples for training the surrogate. In Section 5, we draw the conclusions and point to future research.

2. Theoretical background

We present the preliminaries and define the input random variables in Section 2.1 and output random variables in Section 2.2. Section 2.3 presents the global sensitivity analysis method. We summarize the polynomial dimensional decomposition surrogate in Section 2.4 and the original D-MORPH regression in Section 2.5.

2.1. Input random variables

Let \mathbb{R} , and \mathbb{R}_0^+ denote the real numbers and non-negative real numbers, respectively. For a positive integer N , denote by $\mathbb{A}^N \subseteq \mathbb{R}^N$ a bounded or unbounded sub-domain of \mathbb{R}^N . Let $(\Omega, \mathcal{F}, \mathbb{P})$ be an abstract probability space, with a sample space Ω , a σ -algebra \mathcal{F} on Ω , and a probability measure $\mathbb{P} : \mathcal{F} \rightarrow [0, 1]$. Consider an N -dimensional random vector $\mathbf{X} := (X_1, \dots, X_N)^\top : \Omega \rightarrow \mathbb{A}^N$ that models the input uncertainties. We refer to \mathbf{X} as the random input vector or the input random variables. Denote by $F_{\mathbf{X}}(\mathbf{x}) := \mathbb{P}[\cap_{i=1}^N \{X_i \leq x_i\}]$ the joint distribution function of \mathbf{X} . In this work, we assume that the input random variables in \mathbf{X} are independent so that the joint probability density function is $f_{\mathbf{X}}(\mathbf{x}) := \prod_{k=1}^N f_k(X_k)$. Here, $f_k(X_k)$ is the marginal probability density function of X_k defined on the probability space $(\Omega_k, \mathcal{F}_k, \mathbb{P}_k)$. For $(\Omega, \mathcal{F}, \mathbb{P})$, the image probability space is $(\mathbb{A}^N, \mathcal{B}^N, f_{\mathbf{X}}(\mathbf{x})d\mathbf{x})$, where \mathbb{A}^N is the image of Ω under the mapping $\mathbf{X} : \Omega \rightarrow \mathbb{A}^N$ and $\mathcal{B}^N := \mathcal{B}(\mathbb{A}^N)$ is the Borel σ -algebra on $\mathbb{A}^N \subset \mathbb{R}^N$.

2.2. Output random variables

Given an input random vector \mathbf{X} with a known probability density function $f_{\mathbf{X}}(\mathbf{x})$ on $\mathbb{A}^N \subseteq \mathbb{R}^N$, denote by $Y = y(\mathbf{X})$ a real-valued, square-integrable function on (Ω, \mathcal{F}) . In this work, we assume that the output function (or quantity of interest) y belongs to the weighted L^2 space

$$\left\{ y : \mathbb{A}^N \rightarrow \mathbb{R} : \int_{\mathbb{A}^N} |y(\mathbf{x})|^2 f_{\mathbf{X}}(\mathbf{x}) d\mathbf{x} < \infty \right\}.$$

If there is more than one output, then each component is associated with a measurement function y_i , $i = 1, 2, \dots$. The generalization for a multivariate output random vector is straightforward.

2.3. Global sensitivity analysis

We review variance-based methods for global sensitivity analysis followed by a brief explanation of how to use the polynomial dimensional decomposition surrogate for variance-based sensitivity analysis.

2.3.1. ANalysis Of VArance (ANOVA) dimensional decomposition

The ANOVA dimensional decomposition assesses the effect of inputs \mathbf{X} on an output $y(\mathbf{X})$. The dimensional decomposition can be expressed as

$$\begin{aligned} y(\mathbf{X}) = & y_0 + \sum_{i=1}^N y_i(X_i) + \sum_{i_1=1}^{N-1} \sum_{i_2=i_1+1}^N y_{i_1 i_2}(X_{i_1}, X_{i_2}) + \cdots \\ & + \sum_{i_1=1}^{N-s+1} \cdots \sum_{i_s=i_{s-1}+1}^N y_{i_1 \dots i_s}(X_{i_1}, \dots, X_{i_s}) + \cdots + y_{12 \dots N}(X_1, \dots, X_N), \end{aligned} \quad (1)$$

where the component functions $y_{i_1, \dots, i_s}(x_{i_1}, \dots, x_{i_s})$ for $1 \leq i_1 < \dots < i_s \leq N$ and $s = 1, \dots, N$ are defined as

$$\begin{aligned} y_0 &:= \int_{\mathbb{R}^N} y(\mathbf{x}) f_{\mathbf{X}}(\mathbf{x}) d\mathbf{x}, \\ y_i(x_i) &:= \int_{\mathbb{R}^{N-1}} y(\mathbf{x}) \prod_{j \neq i} f_{X_j}(x_j) dx_j - y_0, \\ y_{i_1 i_2}(x_{i_1}, x_{i_2}) &:= \int_{\mathbb{R}^{N-2}} y(\mathbf{x}) \prod_{j \neq \{i_1, i_2\}} f_{X_j}(x_j) dx_j - y_{i_1}(x_{i_1}) - y_{i_2}(x_{i_2}) - y_0, \\ y_{i_1 \dots i_s}(X_{i_1}, \dots, X_{i_s}) &:= \int_{\mathbb{R}^{N-s}} y(\mathbf{x}) \prod_{j \neq \{i_1, \dots, i_s\}} f_{X_j}(x_j) dx_j - \sum_{j_1 < \dots < j_{s-1} \subset \{i_1, \dots, i_s\}} y_{j_1 \dots j_{s-1}}(x_{j_1}, \dots, x_{j_{s-1}}) \\ &\quad - \sum_{j_1 < \dots < j_{s-2} \subset \{i_1, \dots, i_s\}} y_{j_1 \dots j_{s-2}}(x_{j_1}, \dots, x_{j_{s-2}}) - \cdots - \sum_{j \subset \{i_1, \dots, i_s\}} y_j(x_j) - y_0. \end{aligned}$$

These component functions satisfy orthogonal properties such that

$$\int_{\mathbb{R}^N} y_{i_1 \dots i_s}(x_{i_1}, \dots, x_{i_s}) f_{\mathbf{X}}(\mathbf{x}) d\mathbf{x} = 0, \quad \int_{\mathbb{R}^N} y_{i_1 \dots i_s}(x_{i_1}, \dots, x_{i_s}) y_{i_1 \dots i_t}(x_{i_1}, \dots, x_{i_t}) f_{\mathbf{X}}(\mathbf{x}) d\mathbf{x} = 0, \quad (2)$$

where $i_1, \dots, i_s \neq i_1, \dots, i_t$ for $1 \leq s \leq N$ and $1 \leq t \leq N$. Applying the ANOVA dimensional decomposition in (1) and the orthogonal properties in (2) to the variance of the quantity of interest, $\sigma_y = \int_{\mathbb{R}^N} (y(\mathbf{x}) - y_0)^2 f_{\mathbf{X}}(\mathbf{x}) d\mathbf{x}$, results in the partitioning of the variance of $y(\mathbf{X})$. This is used for deriving the variance-based sensitivity method, as introduced in the following section.

2.3.2. Variance-based sensitivity analysis

For $\mathcal{V} \subseteq \{1, \dots, N\}$, let the $|\mathcal{V}|$ -variate global sensitivity index of a random output $Y = y(\mathbf{X})$ be

$$S_{\mathcal{V}} := \frac{\sigma_{\mathcal{V}}^2}{\sigma_y^2}, \quad \sigma_y > 0, \quad (3)$$

where $\sigma_{\mathcal{V}}^2$ is the variance of $y_{i_1 \dots i_{|\mathcal{V}|}}(X_{i_1}, \dots, X_{i_{|\mathcal{V}|}})$ defined above. This non-negative sensitivity index reflects the fraction of the variance of $y(\mathbf{X})$ contributed by the inputs $X_{i_1}, \dots, X_{i_{|\mathcal{V}|}}$.

2.4. Polynomial dimensional decomposition surrogate

For any output function $y(\cdot)$ that is square-integrable on the probability space $(\Omega, \mathcal{F}, \mathbb{P})$ there exists a Fourier-polynomial expansion, called *polynomial dimensional decomposition (PDD)*, given by

$$y(\mathbf{X}) = y_0 + \sum_{\emptyset \neq \mathcal{U} \subseteq \{1, \dots, N\}} \sum_{\mathbf{j}_{\mathcal{U}} \in \mathbb{N}^{|\mathcal{U}|}} c_{\mathcal{U}, \mathbf{j}_{\mathcal{U}}} \Psi_{\mathcal{U}, \mathbf{j}_{\mathcal{U}}}(\mathbf{X}_{\mathcal{U}}), \quad c_{\mathcal{U}, \mathbf{j}_{\mathcal{U}}} := \int_{\mathbb{A}^N} y(\mathbf{x}) \Psi_{\mathcal{U}, \mathbf{j}_{\mathcal{U}}}(\mathbf{x}_{\mathcal{U}}) f_{\mathbf{X}}(\mathbf{x}) d\mathbf{x},$$

where $c_{\mathcal{U}, \mathbf{j}_{\mathcal{U}}}$ are the expansion coefficients and the multivariate orthonormal polynomial is defined as $\Psi_{\mathcal{U}, \mathbf{j}_{\mathcal{U}}}(\mathbf{X}_{\mathcal{U}}) = \prod_{i \in \mathcal{U}} \Psi_{i, j_i}(X_i)$, where Ψ_{i, j_i} is a univariate orthonormal polynomial in X_i of degree j_i that is consistent with the probability measure $f_{X_i}(X_i)dx_i$. The full PDD contains an infinite number of expansion coefficients. In practice, the PDD must be truncated to have a finite number of expansion coefficients. A straightforward approach is to retain the degrees of interaction among input variables less than or equal to S . For example, when $S = 1$ and $S = 2$, the PDD includes at most univariate and bivariate polynomials, respectively. We then preserve the degree or order m of the polynomial expansion such that $S \leq m < \infty$. This truncation results in an S -variate, m th-order PDD approximation, i.e.,

$$y_{S,m}(\mathbf{X}) := y_0 + \sum_{\substack{\emptyset \neq \mathcal{U} \subseteq \{1, \dots, N\} \\ 1 \leq |\mathcal{U}| \leq S}} \sum_{\substack{\mathbf{j}_{\mathcal{U}} \in \mathbb{N}^{|\mathcal{U}|} \\ |\mathcal{U}| \leq |\mathbf{j}_{\mathcal{U}}| \leq m}} c_{\mathcal{U}, \mathbf{j}_{\mathcal{U}}} \Psi_{\mathcal{U}, \mathbf{j}_{\mathcal{U}}}(\mathbf{X}_{\mathcal{U}}) \approx y(\mathbf{X}).$$

We can arrange the elements of the basis in any order, such that

$$\{\Psi_{\mathcal{U}, \mathbf{j}_{\mathcal{U}}}(\mathbf{X}_{\mathcal{U}}) : 1 \leq |\mathcal{U}| \leq S, |\mathcal{U}| \leq |\mathbf{j}_{\mathcal{U}}| \leq m\} = \{\Psi_2(\mathbf{X}), \dots, \Psi_L(\mathbf{X})\}, \quad \Psi_1(\mathbf{X}) = 1,$$

where $\Psi_i(\mathbf{X})$ represents the i th basis function in the truncated PDD approximation. With this, the PDD approximation can be rewritten as

$$y_{S,m}(\mathbf{X}) = \sum_{i=1}^L c_i \Psi_i(\mathbf{X}) \quad (4)$$

where $c_i \in \mathbb{R}$ is the corresponding expansion coefficient for $i = 1, \dots, L$ and where

$$L = L(S, N, m) = 1 + \sum_{s=1}^S \binom{N}{s} \binom{m}{s}. \quad (5)$$

We can use the S -variate, m th-order PDD approximation to estimate the global sensitivity index $S_{\mathcal{V}}$ from (3) for $\emptyset \neq \mathcal{V} \subseteq \mathcal{U}$ as

$$S_{\mathcal{V}} \approx \sum_{\substack{\mathbf{j}_{\mathcal{V}} \in \mathbb{N}^{|\mathcal{V}|} \\ |\mathcal{V}| \leq |\mathbf{j}_{\mathcal{V}}| \leq m}} c_{\mathcal{V}, \mathbf{j}_{\mathcal{V}}}^2 \bigg/ \sum_{\substack{\emptyset \neq \mathcal{U} \subseteq \{1, \dots, N\} \\ 1 \leq |\mathcal{U}| \leq S}} \sum_{\substack{\mathbf{j}_{\mathcal{U}} \in \mathbb{N}^{|\mathcal{U}|} \\ |\mathcal{U}| \leq |\mathbf{j}_{\mathcal{U}}| \leq m}} c_{\mathcal{U}, \mathbf{j}_{\mathcal{U}}}^2.$$

2.5. Diffeomorphic Modulation under Observable Response Preserving Homotopy (D-MORPH) regression

The authors in [15, 16] introduce the D-MORPH regression to solve an underdetermined linear system, i.e., a system with more unknown parameters than training samples. Consider $\mathbf{x}^{(l)} = (x_1^{(l)}, \dots, x_N^{(l)})^\top$ for $l = 1, \dots, M$, obtained by (quasi) Monte Carlo or Latin hypercube sampling with corresponding probability $f_{\mathbf{X}}(\mathbf{x})$. Given $M < L$, the expansion coefficients $\mathbf{c} = (c_1, c_2, \dots, c_L)^\top \in \mathbb{R}^L$ in (4) of the PDD approximation can be obtained by solving an underdetermined linear system

$$\underbrace{\begin{bmatrix} \Psi_1(\mathbf{x}^{(1)}) & \dots & \Psi_L(\mathbf{x}^{(1)}) \\ \vdots & \ddots & \vdots \\ \Psi_1(\mathbf{x}^{(M)}) & \dots & \Psi_L(\mathbf{x}^{(M)}) \end{bmatrix}}_{=: \mathbf{A}} \underbrace{\begin{bmatrix} c_1 \\ c_2 \\ \vdots \\ c_L \end{bmatrix}}_{\mathbf{c}} = \underbrace{\begin{bmatrix} y(\mathbf{x}^{(1)}) \\ y(\mathbf{x}^{(2)}) \\ \vdots \\ y(\mathbf{x}^{(M)}) \end{bmatrix}}_{=: \mathbf{b}}. \quad (6)$$

Assembling the right-hand side requires costly simulations, hence it is desirable to minimize the number of M . Since there exists an infinite number of solutions for \mathbf{c} that satisfy (6), a manifold $\mathcal{M} \subseteq \mathbb{R}^L$ is constructed to include all potential solutions. The D-MORPH regression aims to obtain the optimal solution \mathbf{c} within \mathcal{M} , by minimizing certain undesirable properties of \mathbf{c} .

Consider $\mathbf{A} \in \mathbb{R}^{M \times L}$ with rank $r < L \leq M$ so that by the singular value decomposition

$$\mathbf{A} = \mathbf{H} \begin{bmatrix} \mathbf{R}_r & \mathbf{0} \\ \mathbf{0} & \mathbf{0} \end{bmatrix} \mathbf{K}^\top, \quad (7)$$

where, \mathbf{H} and \mathbf{K} are $M \times M$ and $L \times L$ orthogonal matrices, respectively, while \mathbf{R}_r is a nonsingular $r \times r$ diagonal matrix. The generalized inverse of the matrix \mathbf{A} is obtained as $\mathbf{A}^+ = \mathbf{K} \begin{bmatrix} \mathbf{R}_r^{-1} & \mathbf{0} \\ \mathbf{0} & \mathbf{0} \end{bmatrix} \mathbf{H}^\top$. Here, $\mathbf{A}^+ \in \mathbb{R}^{L \times L}$ satisfies the four Moore-Penrose conditions: $\mathbf{A}\mathbf{A}^+\mathbf{A} = \mathbf{A}$, $\mathbf{A}^+\mathbf{A}\mathbf{A}^+ = \mathbf{A}^+$, $(\mathbf{A}\mathbf{A}^+)^\top = \mathbf{A}\mathbf{A}^+$, $(\mathbf{A}^+\mathbf{A})^\top = \mathbf{A}^+\mathbf{A}$.

Consider $t \in \mathbb{R}_0^+$ as a scalar variable that is used to parametrize the vector $\mathbf{a}(t) = (a_1(t), \dots, a_L(t))^\top \in \mathbb{R}^L$ of all potential solutions of PDD expansion coefficients. Let $\mathbf{u}(t)$ denote an arbitrary function vector in \mathbb{R}^L . The set of potential solutions within \mathcal{M} is expressed as

$$\mathbf{a}(t) = \mathbf{A}^+\mathbf{b} + (\mathbf{I}_L - \mathbf{A}^+\mathbf{A})\mathbf{u}(t). \quad (8)$$

The first part of the solution $\mathbf{A}^+\mathbf{b}$ in (8) is an initial estimate for \mathbf{c} , akin to the standard least-squares solution when the regularization term is ignored. We proceed to discuss the second term in (8). Define

$$\Phi := (\mathbf{I}_L - \mathbf{A}^+\mathbf{A}) \in \mathbb{R}^{L \times L} \quad \text{and} \quad \mathbf{v}(t) := \frac{d\mathbf{u}(t)}{dt} \in \mathbb{R}^L. \quad (9)$$

From the Moore-Penrose conditions, we can show that Φ is an orthogonal projector with the properties $\Phi^2 = \Phi$ and $\Phi^\top = \Phi$. When differentiating (8) with respect to t and using (9), we obtain

$$\frac{d\mathbf{a}(t)}{dt} = \Phi \mathbf{v}(t). \quad (10)$$

In the standard D-MORPH regression, one defines a quadratic cost function $\mathcal{K}(\mathbf{a}(t)) \in \mathbb{R}_0^+$ and subsequently minimizes it, i.e., the original D-MORPH solves

$$\min_{t \in \mathbb{R}} \left\{ \mathcal{K}(\mathbf{a}(t)) = \frac{1}{2} \mathbf{a}^\top(t) \mathbf{D} \mathbf{a}(t) \right\}. \quad (11)$$

Here, \mathbf{D} is an $L \times L$ real-valued, symmetric, non-negative definite matrix, so that the coefficients $a_i(t)$, $i = 1, \dots, L$, contract during the D-MORPH iterations at rates depending on the elements of \mathbf{D} . If \mathbf{D} is a diagonal matrix, then relatively larger values may be assigned to appropriate diagonal entries to suppress contributions from high-order basis functions of PDD. In (10), we select

$$\mathbf{v}(t) = -\frac{\partial \mathcal{K}(\mathbf{a}(t))}{\partial \mathbf{a}(t)}. \quad (12)$$

Using the chain rule and properties of the projector Φ , it can be shown that

$$\frac{d\mathcal{K}(\mathbf{a}(t))}{dt} = - \left(\Phi \frac{\partial \mathcal{K}(\mathbf{a}(t))}{\partial \mathbf{a}(t)} \right)^\top \left(\Phi \frac{\partial \mathcal{K}(\mathbf{a}(t))}{\partial \mathbf{a}(t)} \right) \leq 0. \quad (13)$$

According to (13), the quadratic cost function $\mathcal{K}(\mathbf{a}(t))$ monotonically decreases as t increases. Com-

binning (10), (11), and (12) results in an initial-value problem governed by the differential equation

$$\frac{d\mathbf{a}(t)}{dt} = -\Phi\mathbf{D}\mathbf{a}(t), \quad \mathbf{a}(0) = \mathbf{A}^+\mathbf{b}. \quad (14)$$

From (14), a transient solution is derived analytically, such that

$$\mathbf{a}(t) = \exp(-t\Phi\mathbf{D})\mathbf{a}(0) = \exp(-t\Phi\mathbf{D})\mathbf{A}^+\mathbf{b}. \quad (15)$$

The singular value of decomposition of $\Phi\mathbf{D}$ is

$$\Phi\mathbf{D} = \mathbf{E} \begin{bmatrix} \mathbf{T}_r & \mathbf{0} \\ \mathbf{0} & \mathbf{0} \end{bmatrix} \mathbf{F}^\top, \quad (16)$$

with \mathbf{T}_r representing an $r \times r$ diagonal matrix with nonzero entries. By taking the limit $t \rightarrow \infty$, the final D-MORPH solution is

$$\bar{\mathbf{c}} = \lim_{t \rightarrow \infty} \mathbf{a}(t) = \mathbf{F}_{L-r}(\mathbf{E}_{L-r}^\top \mathbf{F}_{L-r})^{-1} \mathbf{E}_{L-r}^\top \mathbf{A}^+\mathbf{b}, \quad (17)$$

where $\bar{\mathbf{c}} = (\bar{c}_1, \dots, \bar{c}_L)^\top$ with $\bar{c}_i \in \mathbb{R}$, $i = 1, \dots, L$, representing the expansion coefficients of PDD by the original D-MORPH regression and matrices \mathbf{E}_{L-r} and \mathbf{F}_{L-r} are constructed from the last $L - r$ columns of matrices \mathbf{E} and \mathbf{F} from (16).

3. A PDD surrogate obtained from a novel D-MORPH regression

We propose a new D-MORPH regression method to train the PDD surrogate in the limited data setting where we define a new cost function for the D-MORPH regression that includes a sparse Lasso solution. This method results in more robustness to variations in the inputs to the QoI while maintaining the training data fit. Section 3.1 presents the challenges encountered when solving underdetermined systems for PDD. In Section 3.2, we propose the novel Lasso-based D-MORPH regression.

3.1. Challenges in solving underdetermined systems for PDD and Lasso regression

The standard PDD surrogate (detailed in Section 2.4) uses the ANOVA decomposition, and thus effectively truncates the basis functions that model higher-order interactions. The PDD surrogate thus mitigates the curse of dimensionality compared to the polynomial chaos expansion surrogate when the QoI is defined via a large number (N) of inputs or is heavily nonlinear so that it requires a large degree (m) in the truncation of PDD. Nevertheless, the PDD surrogate can still require several hundreds to thousands of training samples. Acquiring such a large number of training samples can be computationally prohibitive. For example, assume that we require 500 training samples for a bivariate ($S = 2$) tenth-order ($m = 10$) PDD approximation of five ($N = 5$) random inputs to calculate the PDD expansion coefficients via a conventional regression method (e.g., standard least squares). If each sample requires a simulation that takes 24 CPU hours, then the process would take 12,000 hours = 500×24 hours. For applications such as char combustion—the focus herein—we need to reduce the number of required training samples.

We thus consider an underdetermined linear system for the expansion coefficients \mathbf{c} of an S -variate m th-order PDD approximation in (6). When using the D-MORPH regression, the solution can be highly sensitive to the selection of the weight values in \mathbf{D} of (14). The strategies for selecting weights in [15, 16] are specific to a particular problem. In this work, we aim to generalize the strategy for selecting weights to work for different problems. Another option is to solve a Lasso regression

$$\min_{\mathbf{c} \in \mathbb{R}^L} \left\{ (\mathbf{b} - \mathbf{A}\mathbf{c})^\top (\mathbf{b} - \mathbf{A}\mathbf{c}) + k \sum_{i=1}^L |c_i| \right\}, \quad (18)$$

where k is a positive real number. The second term of (18) is a regularization term that penalizes the L1 norm of the PDD's expansion coefficients, producing sparse solutions for underdetermined systems. However, Lasso introduces a bias into the estimates to reduce the variance (the classical bias/variance trade-off in statistics). Due to the nature of the L1 penalty, the Lasso cannot select more coefficients than the number of training samples.

In the following section, we introduce a new D-MORPH regression method that combines the benefits of both the D-MORPH and the Lasso regression. The new method provides accurate PDD expansion coefficients from an underdetermined linear system (6). This is possible as the new regression method improves the robustness of the D-MORPH solution to variations in input values or weight values and overcomes the disadvantages of the Lasso regression.

3.2. Novel Lasso-based D-MORPH regression

To compute the PDD expansion coefficients \mathbf{c} for (4), we solve a linear system (6). We consider the limited data setting, where the system for the unknown regression coefficients is underdetermined, i.e., $M < L$.

3.2.1. Cost function

We define a new cost function that includes the difference between an L -column vector of a potential solution $\mathbf{a}(t) = (a_1(t), \dots, a_L(t))^T$ of PDD expansion coefficients and an L -column vector of the Lasso solution $\mathbf{c}_0 = (c_{0,1}, \dots, c_{0,L})^T$. We include in this cost a second term to penalize the difference between a potential solution $\mathbf{a}(t)$ and a prior D-MORPH solution $\mathbf{c}_1 = (c_{1,1}, \dots, c_{1,L})^T$. The new D-MORPH regression aims to minimize the cost function $\check{\mathcal{K}}(\mathbf{a}(t))$, i.e.,

$$\min_{t \in \mathbb{R}} \left\{ \check{\mathcal{K}}(\mathbf{a}(t)) = \frac{\lambda}{2} (\mathbf{a}(t) - \mathbf{c}_0)^T \mathbf{W} (\mathbf{a}(t) - \mathbf{c}_0) + \frac{1-\lambda}{2} (\mathbf{a}(t) - \mathbf{c}_1)^T \mathbf{W} (\mathbf{a}(t) - \mathbf{c}_1) \right\} \quad (19)$$

with a non-negative real-valued weight $\lambda \in [0, 1]$. Here, $\mathbf{W} = \text{diag}[1/(c_{1,1} + \epsilon), \dots, 1/(c_{1,L} + \epsilon)]$ is an L -dimensional diagonal matrix, and where $\epsilon \ll 1$. When the elements of \mathbf{c}_1 are smaller, this matrix assigns larger weights to the corresponding elements of $\mathbf{a}(t) - \mathbf{c}_0$ and $\mathbf{a}(t) - \mathbf{c}_1$. As the zero entries of \mathbf{c}_1 have the largest weights, $1/\epsilon$, the corresponding elements of $\mathbf{a}(t)$ are the most strongly constrained to the elements of \mathbf{c}_0 and \mathbf{c}_1 .

3.2.2. Non-homogeneous ordinary differential equation for D-MORPH regression

We perform a D-MORPH regression to minimize the new cost function (19). This way, we combine the advantages of both the D-MORPH and Lasso regression and obtain a more robust solution to the expansion coefficients of the PDD surrogate. With the new cost function (19), we set up a non-homogeneous ordinary differential equation in a similar fashion to (10) and (12) as

$$\frac{d\mathbf{a}(t)}{dt} = -\Phi \mathbf{W} \mathbf{a}(t) + \Phi \mathbf{W} (\lambda \mathbf{c}_0 + (1-\lambda) \mathbf{c}_1), \quad \mathbf{a}(0) = \mathbf{A}^+ \mathbf{b}, \quad (20)$$

which has the solution

$$\mathbf{a}(t) = \exp(-t\Phi \mathbf{W}) \mathbf{A}^+ \mathbf{b} + \int_0^t \exp\{-(t-q)\Phi \mathbf{W}\} \Phi \mathbf{W} (\lambda \mathbf{c}_0 + (1-\lambda) \mathbf{c}_1) dq, \quad (21)$$

where the second term represents the particular solution. Taking the limit $t \rightarrow \infty$, the D-MORPH solution to (6) is $\check{\mathbf{c}} = \lim_{t \rightarrow \infty} \mathbf{a}(t)$, which can be written as

$$\check{\mathbf{c}} = \bar{\mathbf{F}}_{L-r} (\bar{\mathbf{E}}_{L-r}^T \bar{\mathbf{F}}_{L-r})^{-1} \bar{\mathbf{E}}_{L-r}^T \mathbf{A}^+ \mathbf{b} + \bar{\mathbf{F}}_r (\bar{\mathbf{E}}_r^T \bar{\mathbf{F}}_r)^{-1} \bar{\mathbf{E}}_r^T (\bar{\mathbf{T}}_r)^{-1} \Phi \mathbf{W}^{-1} (\lambda \mathbf{c}_0 + (1-\lambda) \mathbf{c}_1). \quad (22)$$

Here, $\bar{\mathbf{E}}_r$ and $\bar{\mathbf{E}}_{L-r}$, $\bar{\mathbf{F}}_r$ and $\bar{\mathbf{F}}_{L-r}$ are constructed from the first r and the last $L - r$ columns of matrices $\bar{\mathbf{E}}$ and $\bar{\mathbf{F}}$, respectively, generated from the singular value decomposition

$$\Phi \mathbf{W} = \bar{\mathbf{E}} \begin{bmatrix} \bar{\mathbf{T}}_r & \mathbf{0} \\ \mathbf{0} & \mathbf{0} \end{bmatrix} \bar{\mathbf{F}}^\top, \quad (23)$$

with Φ representing an orthogonal projector in (9) and $\bar{\mathbf{T}}_r$ representing an $r \times r$ diagonal matrix including nonzero singular values.

3.2.3. Recursive process for improving the D-MORPH solution

We use an iterative process to enhance the D-MORPH solution $\check{\mathbf{c}}$ in (22). Denote the D-MORPH solution at the i th iteration as $\check{\mathbf{c}}^{(i)} = (\check{c}_1^{(i)}, \dots, \check{c}_L^{(i)})^\top$. This is derived from the reformulation of (22) as:

$$\begin{aligned} \check{\mathbf{c}}^{(i)} = & \bar{\mathbf{F}}_{L-r}^{(i-1)} (\bar{\mathbf{E}}_{L-r}^{(i-1)\top} \bar{\mathbf{F}}_{L-r}^{(i-1)})^{-1} \bar{\mathbf{E}}_{L-r}^{(i-1)\top} \mathbf{A}^+ \mathbf{b} + \\ & \bar{\mathbf{F}}_r^{(i-1)} (\bar{\mathbf{E}}_r^{(i-1)\top} \bar{\mathbf{F}}_r^{(i-1)})^{-1} \bar{\mathbf{E}}_r^{(i-1)\top} (\bar{\mathbf{T}}_r^{(i-1)})^{-1} \Phi \text{diag}(\check{\mathbf{c}}^{(i-1)})^{-1} (\lambda \mathbf{c}_0 + (1 - \lambda) \check{\mathbf{c}}^{(i-1)}), \end{aligned} \quad (24)$$

where $\bar{\mathbf{E}}_r^{(i)}$ and $\bar{\mathbf{E}}_{L-r}^{(i)}$, $\bar{\mathbf{F}}_r^{(i)}$ and $\bar{\mathbf{F}}_{L-r}^{(i)}$ are constructed from the first r and the last $L - r$ columns of matrices $\bar{\mathbf{E}}^{(i)}$ and $\bar{\mathbf{F}}^{(i)}$, respectively, generated from the singular value decomposition

$$\Phi \mathbf{W}^{(i-1)} = \bar{\mathbf{E}}^{(i-1)} \begin{bmatrix} \bar{\mathbf{T}}_r^{(i-1)} & \mathbf{0} \\ \mathbf{0} & \mathbf{0} \end{bmatrix} \bar{\mathbf{F}}^{(i-1)\top}, \quad (25)$$

with $\bar{\mathbf{T}}^{(i-1)}$ representing an $r \times r$ diagonal matrix including nonzero singular values. Here, $\mathbf{W}^{(i-1)} = \text{diag}[0, 1/(\check{c}_2^{(i-1)} + \epsilon), \dots, 1/(\check{c}_L^{(i-1)} + \epsilon)]$, where its first element is *zero* and the remaining elements are the reciprocal of $\check{c}_j^{(i-1)}$ for $j = 2, \dots, L$ with $\epsilon \ll 1$.

The initial D-MORPH regression is

$$\check{\mathbf{c}}^{(0)} = \bar{\mathbf{F}}_{L-r} (\bar{\mathbf{E}}_{L-r}^\top \bar{\mathbf{F}}_{L-r})^{-1} \bar{\mathbf{E}}_{L-r}^\top \mathbf{A}^+ \mathbf{b} + \bar{\mathbf{F}}_r (\bar{\mathbf{E}}_r^\top \bar{\mathbf{F}}_r)^{-1} \bar{\mathbf{E}}_r^\top (\bar{\mathbf{T}}_r)^{-1} \Phi \check{\mathbf{c}}_0, \quad (26)$$

where $\bar{\mathbf{E}}_r$ and $\bar{\mathbf{E}}_{L-r}$, $\bar{\mathbf{F}}_r$ and $\bar{\mathbf{F}}_{L-r}$ are constructed from the first r and the last $L - r$ columns of matrices $\bar{\mathbf{E}}$ and $\bar{\mathbf{F}}$, respectively. These matrices are generated from the singular value decomposition

$$\Phi = \bar{\mathbf{E}} \begin{bmatrix} \bar{\mathbf{T}}_r & \mathbf{0} \\ \mathbf{0} & \mathbf{0} \end{bmatrix} \bar{\mathbf{F}}^\top, \quad (27)$$

with $\bar{\mathbf{T}}_r$ representing an $r \times r$ diagonal matrix including nonzero singular values.

4. Global sensitivity analysis by a PDD surrogate

We leverage the new D-MORPH regression PDD surrogate for global sensitivity analysis in the limited data setting. Given a limited computational budget, Section 4.1 presents the complete algorithm of the proposed method for global sensitivity analysis. In Section 4.2, we evaluate the proposed method for global sensitivity analysis using the Ishigami & Homma function. We assess the convergence of the proposed method by comparing its results to the exact sensitivity solutions using the Oakley & O'Hagan function in Section 4.3.

4.1. Complete algorithm for global sensitivity analysis

The flow chart in Figure 1 details the procedure for implementing the PDD surrogate modeling for global sensitivity analysis under a budget constraint. Define $B \in \mathbb{R}_0^+$ as the total computational budget and $B_S \in \mathbb{R}_0^+$ as the computational cost required to obtain a single training sample. The total

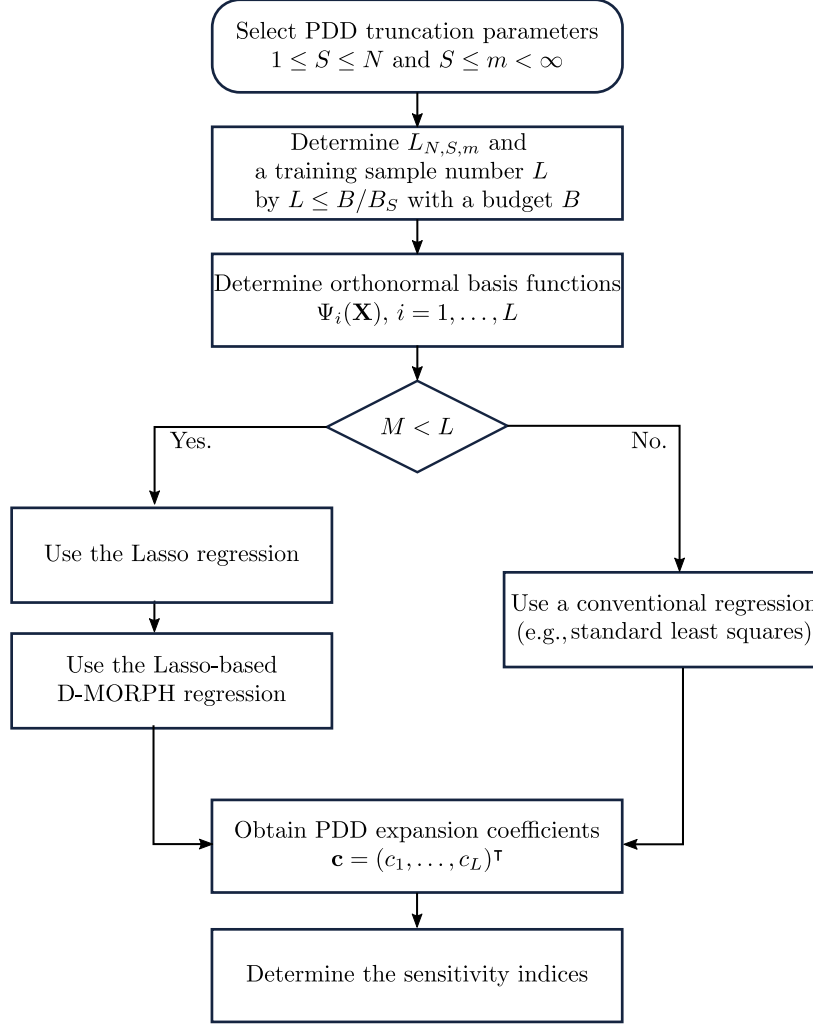


Figure 1: Flow chart for computing the PDD surrogate with the proposed D-MORPH regression for global sensitivity analysis.

cost is $B = M \times B_S$, where M is the number of training samples affordable by the computational budget. We then select the PDD truncation parameters S and m . In this work, we choose $S = 2$ and m ranges from 5 to 11 to attain a target estimate that aligns closely with an unbiased Monte Carlo estimate with M samples. In the limited data setting, $M < L$, we use Lasso regression to obtain the initial \mathbf{c}_0 in (19) followed by the proposed D-MORPH regression to obtain PDD expansion coefficients (22). Otherwise, we have the overdetermined case and can use a conventional regression (e.g., standard least squares). We determine the first and the second sensitivity indices and the total effect sensitivity indices, as detailed in Section 2.3.

4.2. Illustrative example 1: Ishigami & Homma function

This first illustrative example demonstrates that the iterative process improves the accuracy of the D-MORPH solution for the highly nonlinear output with high-order interactions.

Table 1: Exact solutions for the standard deviation and the first-order and the second-order sensitivity indices of Ishigami & Homma function.

	Exact solution	Exact solution ($a = 7, b = 0.1$)
σ_Y (Standard deviation of Y)	$\sqrt{a^2/8 + b\pi^4/5 + b^2\pi^8/18 + 1/2}$	3.720832 ^(a)
S_1 (First-order sobol index for X_1)	$(b\pi^4/5 + b^2\pi^8/50 + 1/2)/\sigma_Y^2$	0.313905 ^(a)
S_2 (First-order sobol index for X_2)	$(a^2/8)/\sigma_Y^2$	0.442411 ^(a)
S_3 (First-order sobol index for X_3)	0	0
$S_{1,2}$ (Second-order sobol index for X_1 and X_2)	0	0
$S_{1,3}$ (Second-order sobol index for X_1 and X_3)	$(8b^2\pi^8/225)/\sigma_Y^2$	0.243684 ^(a)
$S_{2,3}$ (Second-order sobol index for X_2 and X_3)	0	0

a. The exact solution is rounded to six decimal places.

Table 2: Standard deviation and first-order and second-order sensitivity estimates by bivariate ($S = 2$) $m = 11$ th-order PDD approximation using Lasso-based DMORPH regression and Lasso regression, with 59 training samples (30% of the number of unknown expansion coefficients).

Methods	Mean relative error ^a ($K = 30$)				Mean absolute error ^b ($K = 30$)		
	Standard deviation	$S_{\{1\}}$	$S_{\{2\}}$	$S_{\{1,3\}}$	$S_{\{3\}}$	$S_{\{1,2\}}$	$S_{\{2,3\}}$
Lasso-based D-MORPH							
Iteration=0	0.128965	0.057175	0.103271	0.192922	0.002249	0.002876	0.008772
Iteration=20	0.083872	0.035874	0.073809	0.149792	0.001271	0.001382	0.005195
Iteration=30	0.069427	0.028573	0.078167	0.137125	0.000573	0.001464	0.004164
Lasso regression	0.157845	0.064819	0.112890	0.199169	0.001420	0.000820	0.005834

a. The mean relative error over 30 trials is the mean absolute error over 30 trials, normalized by the exact solution.

b. The mean absolute error over 30 trials is used when the exact solution is *zero*.

4.2.1. Problem definition

Consider the Ishigami & Homma function from [7], given as

$$y(\mathbf{X}) = \sin X_1 + a \sin^2 X_2 + b X_3^4 \sin X_1, \quad (28)$$

where X_1, X_2, X_3 are independent and identically distributed uniform input random variables on $[-\pi, +\pi]$, and a and b are real-valued deterministic parameters; we select $a = 7$ and $b = 0.1$. Table 1 reports the exact solutions for the variance and sensitivity indices of the output random variable $Y = y(\mathbf{X})$.

4.2.2. Process of global sensitivity analysis

We select the PDD truncation parameters $S = 2$ and $m = 11$ so that the PDD has $L = 199$ expansion coefficients, see (5). We consider $M = 59$ training samples, which is 30% of $L = 199$. Since the linear system from (6) is underdetermined (i.e., $M < L$), we use the Lasso-based D-MORPH regression and select the weight $\lambda = 0.5$. We then use the obtained expansion coefficients to determine the variance and the first and second-order sensitivity indices, as detailed in Sections 2.3 and 2.4.

4.2.3. Results

Table 2 reports the mean errors (absolute and relative, depending on if we have zero or non-zero reference values) of the bivariate eleventh-order PDD computed by the Lasso-based D-MORPH regression for the standard deviation, the first-order sensitivity indices $S_{\{i\}}$, and the second-order sensitivity indices $S_{\{i,j\}}$, where $i, j = 1, 2, 3$ and $j > i$, compared to the exact solutions in Table 1.

The *mean absolute error* and the *mean relative error* are obtained by

$$\frac{1}{K} \sum_{k=1}^K |\mathcal{Y} - \mathcal{Y}_k| \quad \text{and} \quad \frac{1}{K} \sum_{k=1}^K \left| \frac{\mathcal{Y} - \mathcal{Y}_k}{\mathcal{Y}} \right|,$$

where \mathcal{Y} is an exact solution for the standard deviation or the sensitivities of $y(\mathbf{X})$ and \mathcal{Y}_k is the PDD estimate of \mathcal{Y} at the k th independent trial run. When the exact solution is non-zero, we normalize the mean absolute error with respect to the corresponding exact solution and obtain the mean relative error. As shown in the second through the fourth row of Table 2, increasing the iteration number i of Equation (22) from 0 to 30 decreases the mean errors accordingly. In particular, the mean relative error of the proposed D-MOPRH for the standard deviation decreases by almost 50% from iteration 0 to 30.

We also include the Lasso estimates in the last row of Table 2. It shows that in the standard deviation and most cases of sensitivity indices, the proposed D-MOPRH estimates are more accurate than the Lasso estimates, while they use only 30% of the number of expansion coefficients. Figures 2a

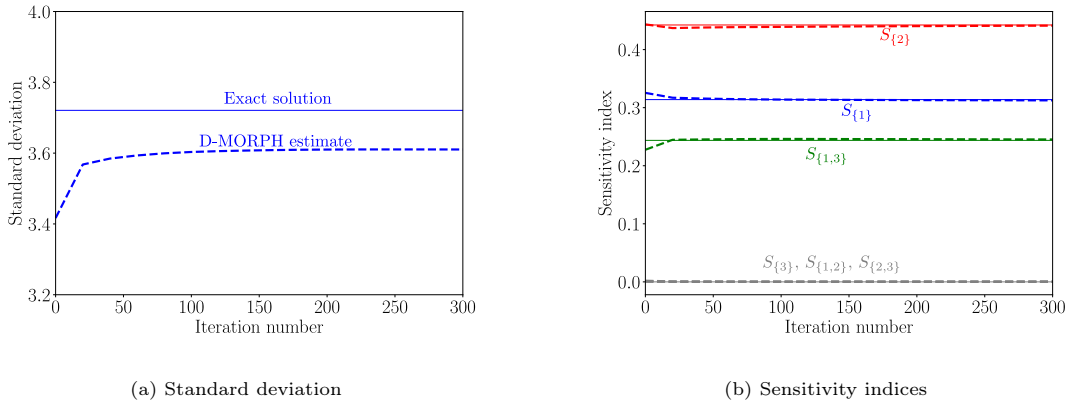


Figure 2: (a) Convergence of PDD estimates computed by a Lasso-based D-MORPH regression for standard deviation; (b) sensitivity indices $S_{\{1\}}, S_{\{2\}}, S_{\{3\}}$ as D-MORPH iteration increases from 0 to 300.

and 2b show the convergence of one realization of PDD estimates computed by the proposed D-MOPRH regression as the iteration number (i) of (22) increases from 0 to 300. In Figure 2a, the standard deviation converges relatively rapidly while there is an existing bias. For example, within 40 iterations, the standard deviation estimate converges from 8.18% to 3.66% error when compared to the exact solution.

The sensitivities also converge rapidly to each of the exact solutions yet without significant bias. For example, within 40 iterations, the first-order sensitivity estimate $S_{\{1\}}$ converges from 3.69% to 0.61% error when compared to the exact solution. After 40 iterations, the convergence rate for the standard deviation and sensitivities ($S_{\{1\}}, S_{\{3\}}, S_{\{1,3\}}$) tends to slow down.

4.3. Illustrative example 2: Oakley & O'Hagan function

In this second example for a relatively high-dimensional global sensitivity analysis problem, we demonstrate the convergence of D-MORPH regression as the number of training samples increases. We also consider different weight values (λ) for the D-MORPH cost function (19).

4.3.1. Problem definition

For global sensitivity analysis, Oakley & O’Hagan [21] introduced a mixture of trigonometric and quadratic polynomial functions as

$$y(\mathbf{X}) = \mathbf{a}_1^\top \mathbf{X} + \mathbf{a}_2^\top \sin \mathbf{X} + \mathbf{a}_3^\top \cos \mathbf{X} + \mathbf{X}^\top \mathbf{M} \mathbf{X},$$

where $\mathbf{X} = (X_1, \dots, X_{15})^\top \in \mathbb{R}^{15}$ is the standard Gaussian input vector ($N = 15$) with mean vector $\mathbb{E}[\mathbf{X}] = (0, \dots, 0)^\top \in \mathbb{R}^{15}$ and covariance matrix $\mathbb{E}[\mathbf{X}\mathbf{X}^\top] - \mathbf{I} \in \mathbb{R}^{15 \times 15}$. Moreover, $\mathbf{a}_i \in \mathbb{R}^{15}$, $i = 1, 2, 3$, and $\mathbf{M} \in \mathbb{R}^{15 \times 15}$ are coefficient vectors and matrix, respectively, obtained from [21]. From the same work, we also obtain the exact solutions for the first-order sensitivities of the fifteen inputs.

4.3.2. Process of global sensitivity analysis

We choose the PDD truncation parameters $S = 2$ and $m = 5$. This results in a PDD with $L = 1,126$ expansion coefficients. We consider three distinct training sample numbers $M = 337$, 563, and 788, which are 30%, 50%, and 70% of the unknown expansion coefficients. Since the linear system in (6) is underdetermined (i.e., $M < L$), we use the Lasso-based D-MORPH regression. For the regression, we select three weights $\lambda = 0.2, 0.6$, and 1.0 .

4.3.3. Results

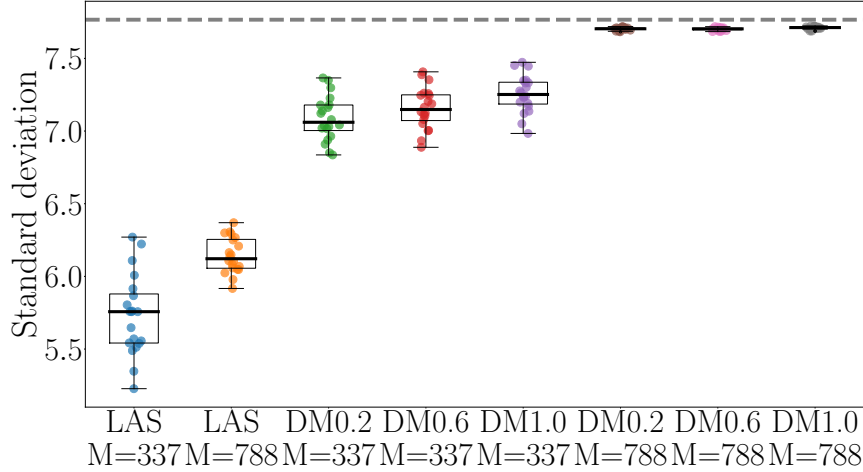


Figure 3: Boxplots of the standard deviation of the random output $y(\mathbf{X})$, estimated by the bivariate fifth-order PDD using the Lasso (LAS) and Lasso-based D-MORPH regressions with weight values $\lambda = 0.2, 0.6, 1.0$ (DM0.2, DM0.6, DM1.0). Two underdetermined systems are considered: $M = 337$ and $M = 788$, which correspond to 30% and 70% of the number ($L = 1,126$) of expansion coefficients. Each regression is repeated 20 times. The exact solution is shown as a gray-dotted line.

Figure 3 shows the standard deviations estimated by the bivariate fifth-order PDD approximations via box plots. These three distinct cases are associated with underdetermined linear systems from (6). Hence, we use a Lasso regression and the proposed Lasso-based D-MORPH regression with three distinct weight values $\lambda = 0.2, 0.6$, and 1.0 , as indicated as ‘LAS’, ‘DM0.2’, ‘DM0.6’, and ‘DM1.0’, respectively, on the x -axis of Figure 3. In the figure, we present the exact solution for the standard deviation with a gray dotted line.

As the number of training samples increases from 337 to 788, the proposed D-MORPH regressions for all weight cases converge more closely to the exact solution compared to the Lasso regression. For example, when $M = 337$, the mean relative errors of the D-MORPH-based estimates compared to the exact standard deviation are 8.74%, 7.84%, and 6.56% for weights 0.2, 0.6, and 1.0, respectively, over 20 experiments. These are 3x more accurate than the Lasso estimates (the mean relative error

26.18% over 20 experiments). The D-MORPH regressions are more robust than the Lasso regression, as shown by the smaller variance of estimates in 20 experiments. As the number of training samples increases, the variance of the D-MORPH regressions also becomes narrower.

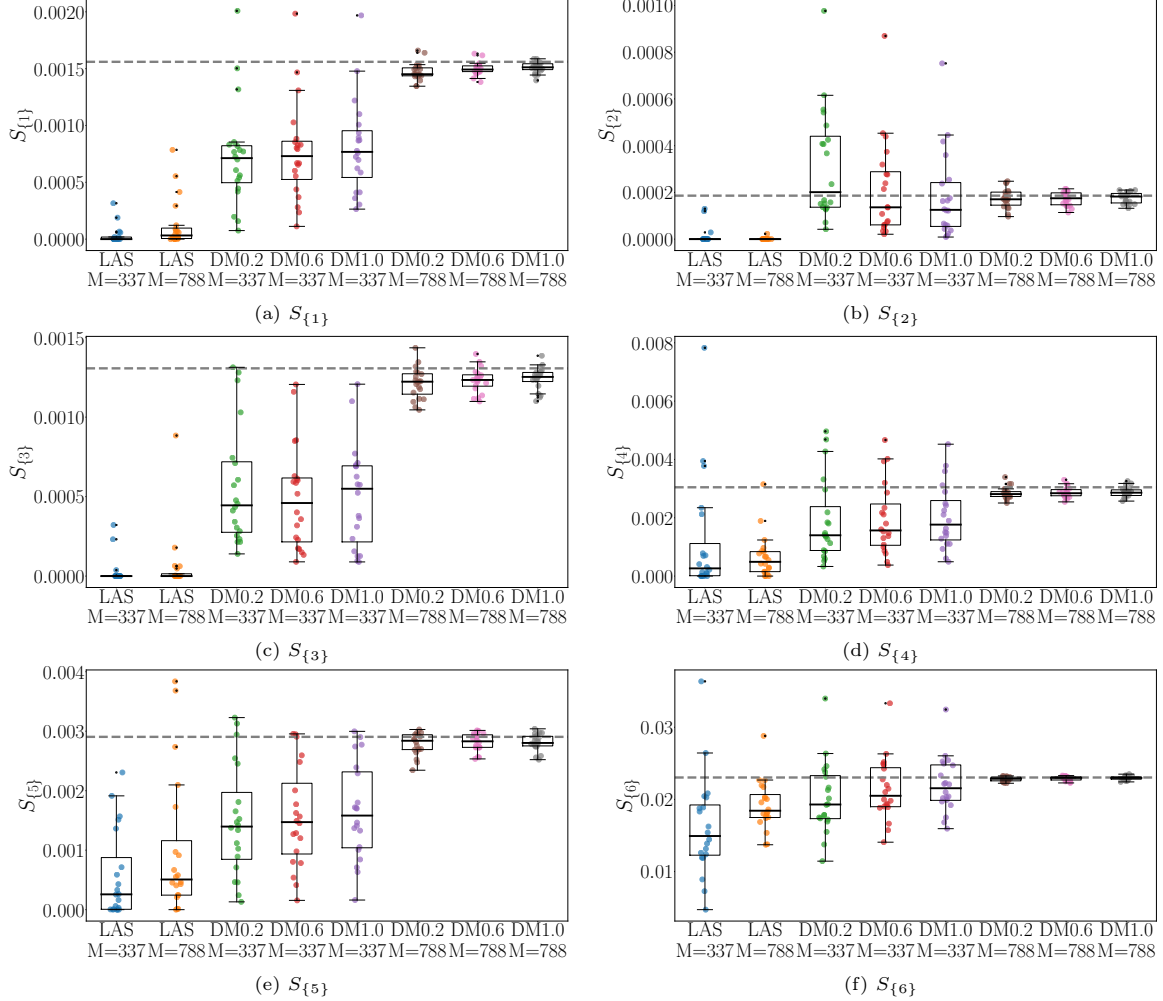


Figure 4: Boxplots of first-order sensitivity indices $S_{\{i\}}$, $i = 1, 2, 3, 4, 5, 6$, of the random output $y(\mathbf{X})$, in (a), (b), (c), (d), (e), (f), respectively, estimated by the bivariate fifth-order PDD using the Lasso (LAS) and Lasso-based D-MORPH regressions with weight values $\lambda = 0.2, 0.6, 1.0$ (DM0.2, DM0.6, DM1.0). Two underdetermined systems are considered: $M = 337$ and $M = 788$, which correspond to 30% and 70% of the number ($L = 1, 126$) of expansion coefficients. Each regression is repeated 20 times. The exact solution is shown as a gray-dotted line.

The graphics in Figure 4 present the estimates by Lasso and the proposed D-MORPH regression for the first-order sensitivity indices $S_{\{i\}}$, $i = 1 - 6$, as they are representative of the other indices as well. In Appendix A, Figures 10 and 11 show additional results for the first-order sensitivity indices $S_{\{i\}}$, $i = 7 - 15$. Taken together, these results demonstrate the superiority of the proposed D-MORPH method for three weight values ($\lambda = 0.2, 0.6, 1.0$) over the Lasso regression in the first-order sensitivity indices, akin to the standard deviation case discussed earlier. Relative to the training sample number L , the estimates of the sensitivity indices computed from the D-MORPH regression-based estimates are less sensitive to the weight value (λ). A weight value of $\lambda = 1$ shows slightly higher accuracy compared to the other weight values.

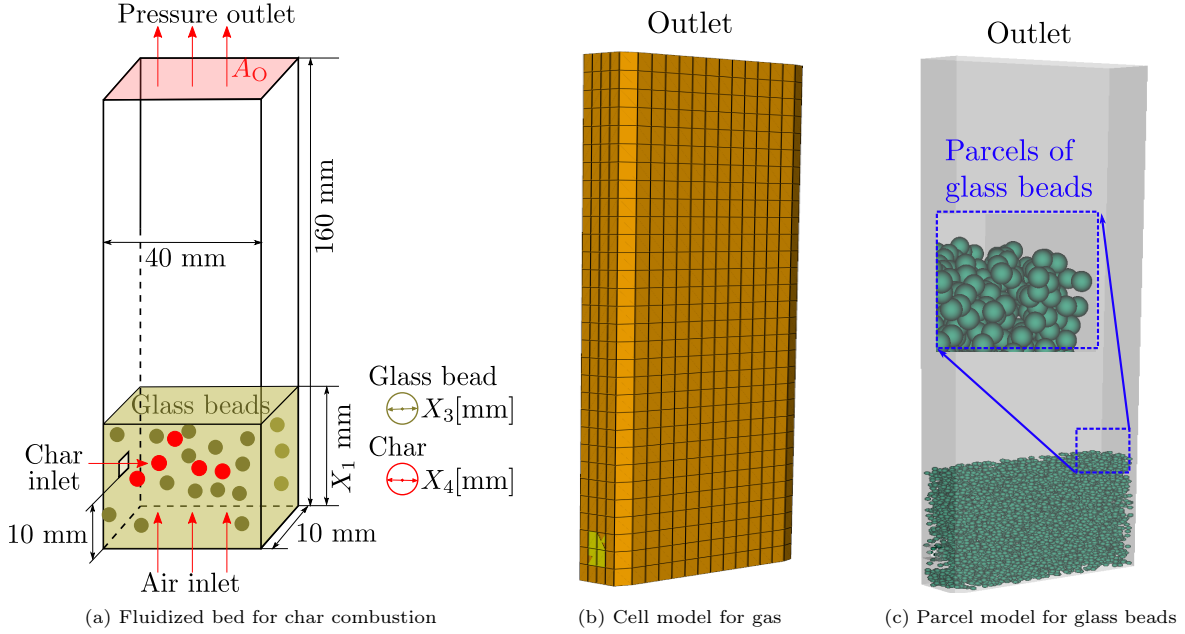


Figure 5: Fluidized bed for char combustion: (a) the schematic diagram shows the geometry and the initial concentration of glass beads with a diameter of X_3 stacked at the boiler’s bottom to a height of X_1 . Char with a diameter of X_4 is fed in through the left side; (b) the cell model used to predict gas behavior consists of 2,520 cells; and (c) the parcel model used to predict solid behavior contains 32,945 parcels.

5. Numerical example: Char combustion

Combustion is a computationally expensive process to simulate. Training surrogate models with such expensive simulation data presents challenges, as one is limited by how much data can be generated with a realistic computational budget. The proposed regression method addresses this computational challenge. In this section, we evaluate the PDD computed by the proposed D-MORPH regression for global sensitivity analysis of an expensive-to-simulate char combustion process with five random input variables.

Sections 5.1 and 5.2 describe the details of the problem and its numerical setting. We validate the simulation model in Section 5.3. Section 5.4 clarifies the quantity of interest for global sensitivity analysis. We present the proposed surrogate modeling results for the mean and the standard deviation of the quantity of interest in Section 5.5. Finally, Section 5.6 shows the results for sensitivity indices via the proposed methods.

5.1. Problem description

Fluidized bed combustion is a combustion technology that burns solid fuels, such as char and biomass, efficiently and with low emissions. The fluidized bed combustion systems can also capture pollutants, such as sulfur dioxide and nitrogen oxides, making them a more environmentally friendly option than traditional combustion methods. To optimize the operational efficiency of fluidized bed combustors, this study focuses on determining the influential parameters that affect the QoI, here a thermal energy, which is computed from combustion simulations. We perform variance-based global sensitivity analysis using the PDD surrogate model with the proposed D-MORPH regression.

Figure 5a shows a geometrical configuration of a fluidized bed for char combustion [31]. The rectangular boiler is a lab-scale model with dimensions of 40 mm \times 160 mm \times 10 mm in width, height, and thickness. In the boiler model, we consider a total of five ($N = 5$) random inputs, so $\mathbf{X} = (X_1, X_2, X_3, X_4, X_5)^T$. The boiler initially contains glass beads stacked at the height X_1 [mm].

Table 3: Properties of the random inputs in a fluidized bed model for char combustion.

Random variable	Property	Mean	COV (%)	Lower boundary	Upper boundary	Probability distribution
X_1	Height of stacked glass beads (m)	0.4	-	0.2	0.6	Uniform
X_2	Air inflow (m/s)	0.825	10	0.425	1.225	Truncated normal
X_3	Diameter of the glass bead particle (m)	8×10^{-4}	-	2×10^{-4}	1.4×10^{-3}	Uniform
X_4	Diameter of the char particle (m)	1×10^{-3}	-	5×10^{-4}	1.5×10^{-3}	Uniform
X_5	Char mass inflow (kg/s)	7.35×10^{-6}	10	1.35×10^{-6}	1.35×10^{-5}	Truncated normal

The char particles are reacted with oxygen from the air at a constant rate of X_2 , generating heat and other products as a char combustion process. The diameter of glass beads is set as X_3 [mm]. Char particles with a diameter of X_4 [mm] are fed into the boiler at a constant rate of X_5 through the 2 mm \times 2 mm char inlet on the left wall. Table 3 lists the random inputs, their interval bounds, and assumptions on their distribution.

5.2. Numerical setting

To predict the combustion behavior in the fluidized bed boiler, we create a numerical model using particle-in-cell (PIC), which we summarize in this section.

5.2.1. Particle-in-cell

In the PIC, the gas phase is modeled using the Eulerian method, which treats the gas phase as continua. Figure 5b shows the computational boiler model used for gas phase simulation, consisting of 2,520 cells. Each cell has six degrees of freedom associated with three velocity components and three scalar variables (temperature, species concentrations, and pressure).

The solids phases of the PIC are modeled using the Lagrangian method, where particles with the same physical properties (e.g., density and diameter) are grouped to effectively track their positions and trajectories. A group of particles with the same physical properties is called a parcel. Different particle diameters with the same materials are viewed as having different physical properties; therefore, they will have separate parcels. Figure 5c shows the parcel model composed of 8,344 parcels for representing the glass beads in the boiler model. Since the PIC method tracks parcels and not particles, PIC provides a significant computational cost reduction. Nevertheless, the combustion simulation is expensive since it incorporates complex particle-scale physics such as chemical reactions, heat transfer, hydrodynamics, and more. The PIC uses the collisional stress model to account for interactions between particles and walls [27]. The collision stress is expressed as

$$\tau = \frac{P_s \varepsilon_s^\beta}{\max(\varepsilon_{cp} - \varepsilon_s, \alpha(1 - \varepsilon_s))},$$

where ε_{cp} is the pre-determined value that describes the maximum possible packing fraction for particles. Here, P_s and β are an empirical pressure constant and an empirical unit-less exponent, and $\alpha = 10^{-9}$ is a non-singularity constant $\alpha \ll 1$. In this work, we select $P_s = 1.0$ and $\beta = 2.0$. We use the open-source software MFIX (version 23.1.1) [3] with an MPI-based parallel computing solver on 15 CPUs (Intel Xeon W-3175X CPU @ 3.10 GHz) for the combustion simulations.

5.2.2. Governing equations for particle-in-cell

In this section, we briefly summarize the governing equations applied in the PIC method to predict the behaviors of both the gas and solid phases. We then introduce the chemical reaction used to predict the char combustion process.

Gas phase model. The conservation of mass, momentum, and internal energy are formulated [20] as

$$\begin{aligned}\frac{\partial}{\partial t}(\varepsilon_g \rho_g) + \frac{\partial}{\partial x_j}(\varepsilon_g \rho_g U_{gj}) &= \sum_{n=1}^{N_g} R_{gn} + (\varepsilon_g \rho_g) + S_g, \\ \frac{\partial}{\partial t}(\varepsilon_g \rho_g U_{gi}) + \frac{\partial}{\partial x_j}(\varepsilon_g \rho_g U_{gj} U_{gi}) &= -\frac{\partial P_g}{\partial x_i} + \frac{\partial \tau_{gij}}{\partial x_j} + \varepsilon_g \rho_g g_i + S_{gi}, \\ \varepsilon_g \rho_g C_{pg} \left[\frac{\partial T_g}{\partial t} + U_{gj} \frac{\partial T_g}{\partial x_j} \right] &= \frac{\partial}{\partial x_j}(\varepsilon_g q_{gj}) + S_g.\end{aligned}$$

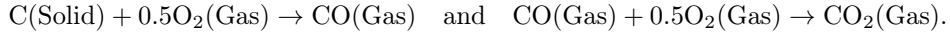
Here, in the gas phase, ε_g is the volume fraction [dimensionless], ρ_g is the density [kg/m³], P_g is the pressure [Pa], T_g is the temperature [K], and C_{pg} is the mixture of specific heat [J/(kg · K)]; S_g is a general user-defined source [kg/(m³ · s)] and S_{gi} is a momentum term [kg/(m² · s²)]. Additionally, N_g is the number of chemical species in the gas phase and R_{gn} is the rate of formation [kmole/(s · m³)] of the n th gas phase, while g_i is the gravitational force [N], U_{ji} is the velocity of gas [m/s] in the j th direction, and τ_{gij} is the stress tensor [Pa] in the gas phase.

Solid phase model. The conservation of mass, momentum, and internal energy are formulated [3] as

$$\begin{aligned}\frac{\partial}{\partial t}(W_p m_p) &= W_p \sum_{n=1}^{N_p} R_{pn}, \\ W_p m_p X_{pn} \frac{\partial U_i}{\partial t} &= W_p (m_p g_i + \frac{m_p}{\varepsilon_s \rho_s} \nabla_{\vec{x}} \tau_p), \\ W_p m_p C_p \frac{\partial T}{\partial t} &= -W_p \sum_{n=1}^{N_p} h_{pn} R_{pn} + S_p.\end{aligned}$$

Here, W_p is the statistical weight [dimensionless] of the particle; for the n th chemical species, R_{pn} is the rate of the production/consumption [kmole/s], X_{pn} is the mass fraction [dimensionless], and h_{pn} is the specific enthalpy [J/kg]. Additionally, C_p is the specific heat [J/(kg · K)] and T is the temperature [K] of the parcel, while S_p is the general source term [kg/(m³ · s)] of the parcel.

Chemical reaction. Char combustion is governed by a heterogeneous gas-solid chemistry. The combustion process generates the two gas products CO and CO₂ from



The collision among particles and the wall leads to the ash falling off from the particles, following an Arrhenius kinetic rate and gas diffusion rate [31], i.e.,

$$\frac{dm_{ci}}{dt} = -\pi d_p^2 p_o \left(\frac{1}{R_{\text{diff}}} + \frac{1}{R_{\text{chem}}} \right)^{-1}, \quad R_{\text{diff}} = \frac{24ShD_o}{d_p RT_m}, \quad R_{\text{chem}} = A_i \exp \left(-\frac{E_i}{RT_p} \right), \quad d_p = \left(\frac{6m_p}{\pi \rho_p} \right)^{1/3}.$$

Here, m_{ci} is the unreacted char mass [kg]; R_{diff} is the gas diffusion rate [m²/s] and R_{chem} is the Arrhenius kinetic rate [s⁻¹]. Also, Sh is the Sherwood number [dimensionless], R is the gas constant [J/(mol · K)], and T is the temperature [K]. Additionally, p_o is the oxygen partial pressure [Pa] and D_o is the oxygen-nitrogen mixture diffusion coefficient [m²/s], while d_p is the particle size [m] as it shrinks due to the mass loss.

The homogeneous reaction can be calculated by the law of mass action via the Arrhenius formula,

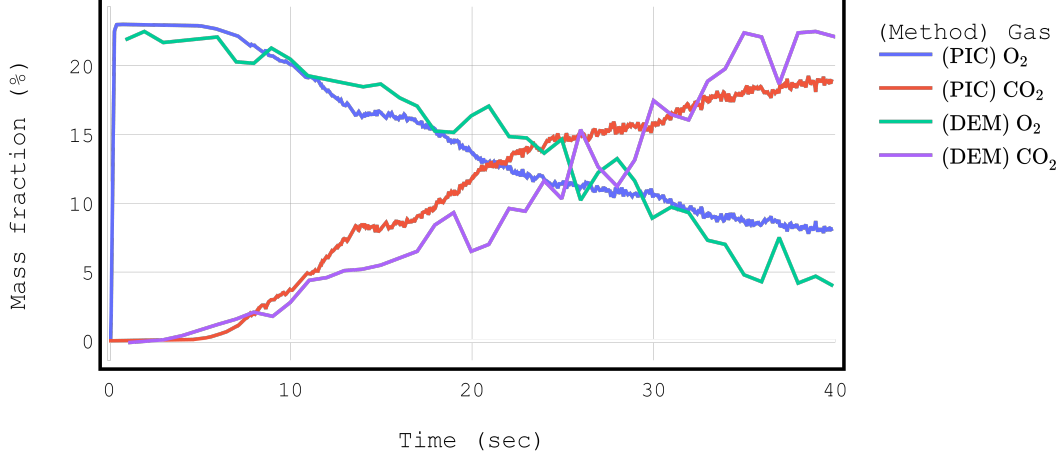


Figure 6: Comparison of the O₂ and CO₂ mass fractions (%) over 40s predicted by the PIC method (used in this work) and the discrete element method (see ‘DEM’ in the figure) results obtained in [31].

proposed by Dryer and Glassman [4], i.e.,

$$r_{co} = 3.98 \times 10^{14} \exp \left(- \frac{1.67 \times 10^5}{RT_g} \right) C_{CO} C_{O_2}^{0.25} C_{H_2O}^{0.5},$$

where C_{CO} , C_{O_2} , and C_{H_2O} are the mass concentrations [kg/m³] of CO, O₂, and H₂O, respectively.

5.3. Validation

In [32, 31], the discrete element method is used to compute the char combustion that couples heat transfer and complex chemical reactions for the boiler geometry configuration shown in Figure 5a. The discrete element method provides highly accurate results as it simulates the individual particle behavior via detailed interactions and dynamics. We thus validate our simulations with the results in [31, Figure 2] obtained by the discrete element method for the time evaluation of the gas mass fractions. For the subsequent validation, we use the mean values of X_1, X_2, \dots, X_5 from [31, Table 1].

Figure 6 presents the simulation results for the mass fractions of CO₂ and O₂ over 40 seconds by the PIC method and the DEM results from [31]. Both methods predict similar changes in the mass fraction of CO₂ and O₂. The CO₂ mass fraction is inversely proportional to the O₂ mass fraction. The Pearson correlation coefficients between the CO₂ and O₂ mass fractions during 1–40 seconds are -0.9999 and -0.9975 from the results by PIC and DEM, respectively. These results indicate that both PIC and DEM demonstrate a strong inverse correlation between the mass fractions of CO₂ and O₂, implying that an increase in CO₂ results in a decrease in O₂. We compute the root-mean-squared error (RMSE) by measuring mass fractions at 5-second intervals over 40 seconds for both methods. The computed RMSE is 2.87 %, indicating that the PIC model is accurate and well-validated compared to the discrete element method model.

5.4. Time integrated quantity of interest

For the global sensitivity analysis, we measure the total thermal energy of a mixed gas from zero to ten seconds as the QoI. We compute the thermal energy as

$$Q(\mathbf{X}) = \int_{t=0}^{t=10} \dot{Q}(\mathbf{X}, t) dt = \int_{t=0}^{t=10} C_p(\mathbf{X}, t) \times \dot{m}(\mathbf{X}, t) \times T_{avg}(\mathbf{X}, t) dt,$$

where $T_{\text{avg}}(\mathbf{X}, t)$ is the average temperature across the outlet's cross-section (see A_O in Figure 5a) at time t and inputs \mathbf{X} , $\dot{m}(\mathbf{X}, t)$ is the mass flow rate at the outlet and $C_p(\mathbf{X}, t)$ is the specific heat capacity of the mixture, i.e., $C_p(\mathbf{X}, t) = \sum_{i=1}^5 C_{pi}(\mathbf{X}, t) \times M_i(\mathbf{X}, t)$. Here, C_{pi} is the specific heat capacity of each gas component in the mixture, and M_i is the mole fraction of each gas component, i.e., $M_1 = 31.9988$ g/mol (O_2), $M_2 = 28.0134$ g/mol (N_2), $M_3 = 28.0104$ g/mol (CO), $M_4 = 44.0098$ g/mol (CO_2), $M_5 = 18.0153$ g/mol (H_2O).

Figure 7a shows the time evolution of thermal energy rate measured at the outlet over 10 seconds. Figure 7b presents the temperature distributions of the cross-section of the boiler at 7 and 9 seconds, as shown in panels A and B, respectively.

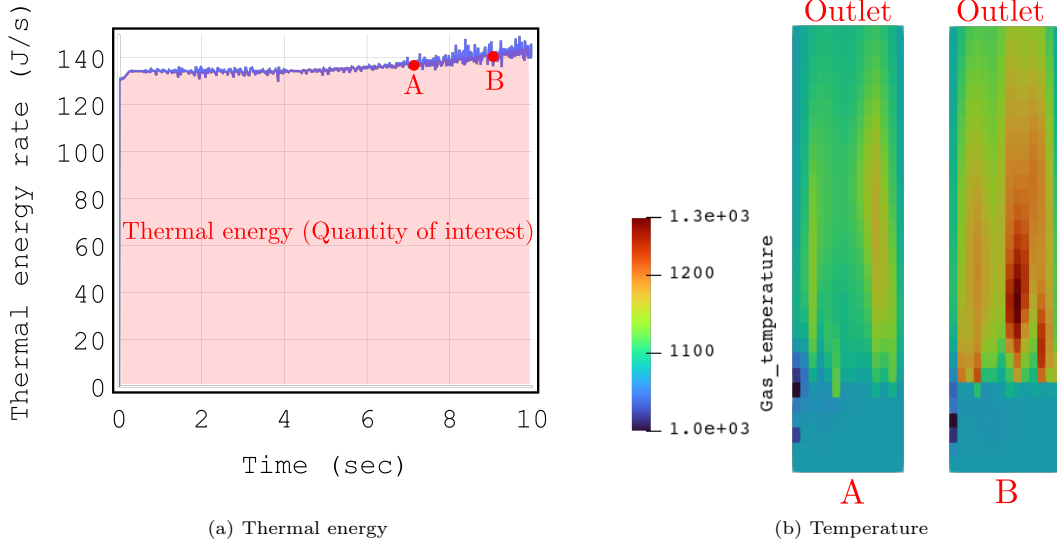


Figure 7: (a) Thermal energy rate (J/s) measured at the outlet over 10 seconds when the mean values of the random inputs $(X_1, X_2, X_3, X_4, X_5)^T$ are used. The measured total thermal energy over 10 seconds (highlighted in red color) is the QoI used for global sensitivity analysis. (b) Temperature distributions at 7 sec (A) and 9 sec (B) in units of Kelvin.

5.5. Surrogate model

We consider a computational budget of 1,200 CPU hours. Within this limit, we obtain 151 training samples for computing the PDD surrogate, i.e., $B=1,200$ hours $>$ 1,192 hours = 151 samples \times 7.9 hours/sample). Given the PDD parameters $S = 2$ and $m = 8$, the surrogate model includes 321 basis functions; we determine the corresponding 321 unknown expansion coefficients via a regression method. With $M = 151$ training samples representing 47% of the $L = 321$ unknown expansion coefficients (leading to an underdetermined linear system in (6)), we use the proposed D-MORPH regression and a standard Lasso regression.

Figure 8a presents boxplots of the standard deviation estimates obtained from a PDD surrogate computed by the proposed D-MORPH regression and a standard Lasso regression over 20 experiments. This figure also includes an unbiased reference obtained by Monte Carlo simulation with 180 samples, shown as in a gray dotted line. For the standard deviation, the proposed D-MORPH results (240.00, 241.64, 246.40) of the three weight cases $\lambda=0.2, 0.6, 1.0$, averaged over 20 experiments, are between 4 – 5x closer to the reference (203.27) by Monte Carlo simulation than the Lasso result (16.47). The standard deviation results of the D-MORPH regression with weights $\lambda=0.2, 0.6, 1.0$ are also close to each other. For the statistical mean, the D-MORPH regression estimates show a relatively higher variance of the estimates over 20 experiments.

Overall, the proposed D-MORPH regression shows superiority to the original Lasso regression for standard deviation estimates. We select the weight of 1.0 to implement global sensitivity analysis, as

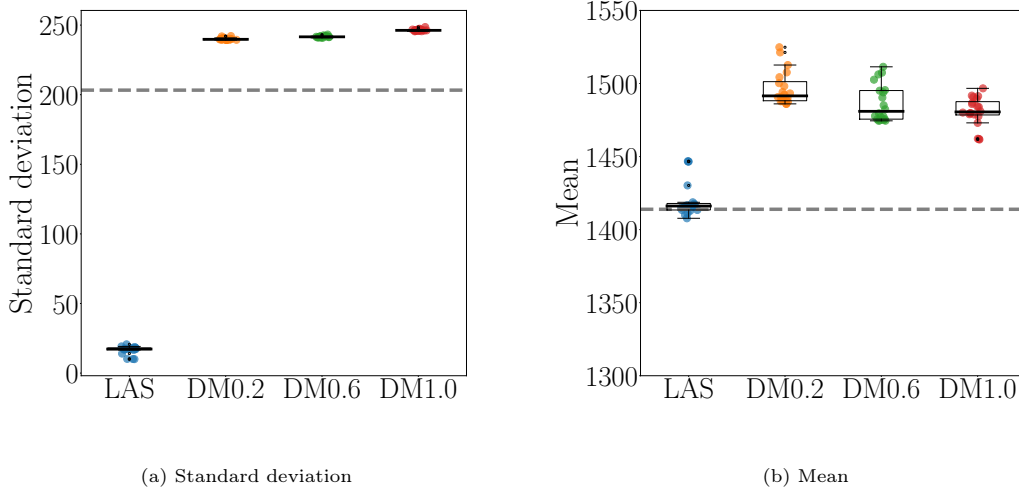


Figure 8: Boxplots of the standard deviation (a) and the mean (b) of the QoI, estimated by the bivariate 8th-order PDD using the Lasso (LAS) and Lasso-based D-MORPH regressions with weight values $\lambda = 0.2, 0.6, 1.0$ (DM0.2, DM0.6, DM1.0). Due to the budget limit (i.e., $M = 151 < L = 321$), we solve the underdetermined system using the Lasso and the proposed Lasso-based D-MORPH regression, repeating this process 20 times. The unbiased Monte Carlo reference with a sample size of 180 is shown as a gray-dotted line.

it shows the least variance of the mean estimates among the remaining weight cases. Although it has the most bias among the three weight cases with respect to the benchmark estimate, we note that the Monte Carlo sampling number (180) used is not enough for accurate benchmark estimates.

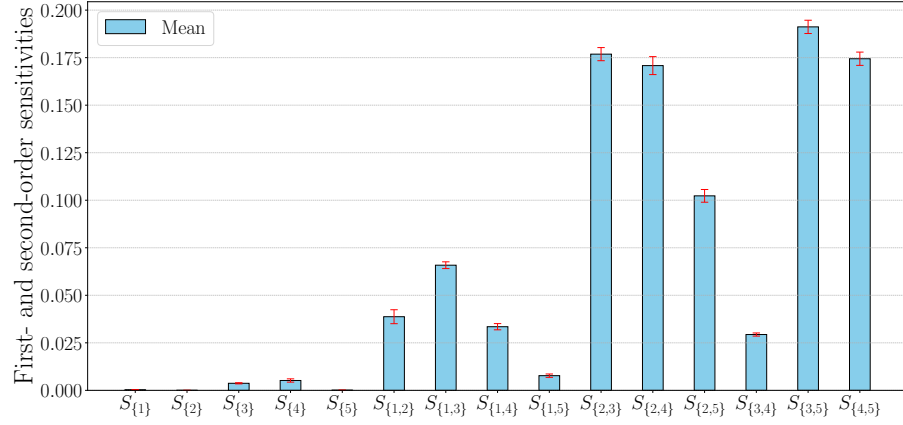
5.6. Global sensitivity analysis

We perform a global sensitivity analysis for the char combustion model via its surrogate described above. Figure 9 presents the global sensitivity analysis results obtained by the PDD surrogate with the proposed D-MORPH regression. In Figure 9a, the bar chart reveals that the first-order sensitivities for inputs X_1 through X_5 are almost negligible, each being less than 1%. Conversely, the second-order sensitivities for all inputs have substantial influence on the QoI. Thus, the joint influence of changing two inputs at the same time can be much larger than only changing one input at a time. Therefore, the Sobol sensitivity method is superior to local sensitivity and Morris screening [19], both of which only capture first-order indices.

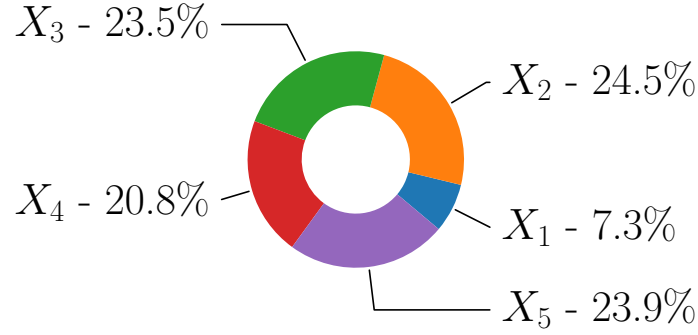
In Figure 9b, the pie chart presents the total effect sensitivities, as a portion of 100%, for inputs X_1 through X_5 . The chart demonstrates that X_2 (air inflow) has the most influence (24.5%) on the QoI, while X_1 (height of stacked glass beads) is the least influential (7.3 %). The other inputs X_3 (diameter of glass beads), X_4 (char diameter), and X_5 (char mass inflow) also significantly impact the QoI, each accounting for over 20% of the total-effect sensitivities. This is important information for system designers and operators. When one optimizes the boiler’s thermal energy, the results from this global sensitivity analysis allow one to prioritize the sensitive inputs, i.e., sizes of the glass beads and char, air inflow, and char mass inflow over the height of the stacked glass beads.

6. Conclusions

We developed a novel D-MORPH regression method to train a PDD surrogate of the quantity of interest in the underdetermined case, which is common in applications where only limited data is available. The new regression method integrates a sparse Lasso solution into the cost function. The difference between the D-MORPH solution and the Lasso solution is minimized iteratively by a



(a) First- and second-order sensitivities



(b) Total effect sensitivities

Figure 9: Estimates of (a) first- and second-order sensitivity indices and (b) total effect sensitivity indices using the PDD surrogate with the proposed D-MORPH regression of weight 1.0. This result shows that X_5 (char mass inflow) is the most influential to the QoI, whereas X_1 (height of the stacked glass beads) is the least influential. The other inputs X_2 (air inflow), X_3 (diameter of glass beads), and X_4 (char diameter) have over 20% impact on the QoI.

D-MORPH regression process. We evaluated the proposed method for global sensitivity analysis in two mathematical functions. A nonlinear function of five random inputs showed that the iterative algorithm improved and converged the D-MORPH solution. In the second mathematical function, we considered fifteen (high-dimensional) random inputs. The results clearly showed that the proposed D-MORPH regression is 3x times more accurate than the standard Lasso regression, and the proposed D-MORPH-based estimates for sensitivities converge as the training sample number increase. We finally demonstrated the versatility and scalability of the PDD surrogate with the proposed D-MORPH regression for global sensitivity analysis of a lab-scale boiler for char combustion. We only used 151 training samples, which are 15% of the data required when using a standard regression method. Consequently, we found four inputs that influence the QoI (thermal energy), showing that the other input is relatively less influential.

This work assumes that input random variables are independent. In practice, there are cases where input variables are dependent or correlated. A potential approach to extend the proposed method to these cases would require the use and development of other surrogates, such as dimensionally decomposed generalized polynomial chaos expansion [12, 14]. This surrogate is more accurate and efficient in handling dependent inputs as the surrogate uses orthonormal polynomial bases for dependent random inputs. Performing a global sensitivity analysis with dependent inputs would then also require a covariance decomposition method instead of the variance-based method.

Acknowledgments

This research was in part financially supported by the Korea Institute for Advancement of Technology (KIAT) through the International Cooperative R&D program (No. P0019804, Digital twin based intelligent unmanned facility inspection solutions). We thank Dr. Kyung Man Kim from Virnect for helpful discussions about the char combustion application.

References

- [1] J. A. Carta, S. Díaz, and A. Castañeda. A global sensitivity analysis method applied to wind farm power output estimation models. *Applied Energy*, 280:115968, 2020.
- [2] K. Cheng, Z. Lu, Y. Zhou, Y. Shi, and Y. Wei. Global sensitivity analysis using support vector regression. *Applied Mathematical Modelling*, 49:587–598, 2017.
- [3] M. A. Clarke and J. M. Musser. The MFIX Particle-in-Cell method (MFIX-PIC) theory guide. Technical report, National Energy Technology Laboratory (NETL), Pittsburgh, PA, Morgantown, 2020.
- [4] F. L. Dryer and I. Glassman. High-temperature oxidation of CO and CH₄. *Symposium (International) on Combustion*, 14(1):987–1003, 1973.
- [5] W. He, G. Li, and Z. Nie. An adaptive sparse polynomial dimensional decomposition based on Bayesian compressive sensing and cross-entropy. *Structural and Multidisciplinary Optimization*, 65(1):26, 2022.
- [6] J. C. Helton and F. J. Davis. Latin hypercube sampling and the propagation of uncertainty in analyses of complex systems. *Reliability Engineering & System Safety*, 81(1):23–69, 2003.
- [7] T. Ishigami and T. Homma. An importance quantification technique in uncertainty analysis for computer models. In *[1990] Proceedings. First international symposium on uncertainty modeling and analysis*, pages 398–403. IEEE, 1990.
- [8] O. Issan, P. Riley, E. Camporeale, and B. Kramer. Bayesian inference and global sensitivity analysis for ambient solar wind prediction. *arXiv preprint arXiv:2305.08009*, 2023.

- [9] A. Jivani, N. Sachdeva, Z. Huang, Y. Chen, B. van der Holst, W. Manchester, D. Iong, H. Chen, S. Zou, X. Huan, et al. Global sensitivity analysis and uncertainty quantification for background solar wind using the alfvén wave solar atmosphere model. *Space Weather*, 21(1):e2022SW003262, 2023.
- [10] Z. Kala. Global sensitivity analysis in stability problems of steel frame structures. *Journal of Civil Engineering and Management*, 22(3):417–424, 2016.
- [11] A. Kiparissides, S. Kucherenko, A. Mantalaris, and E. Pistikopoulos. Global sensitivity analysis challenges in biological systems modeling. *Industrial & Engineering Chemistry Research*, 48(15):7168–7180, 2009.
- [12] D. Lee and B. Kramer. Bi-fidelity conditional value-at-risk estimation by dimensionally decomposed generalized polynomial chaos expansion. *Structural and Multidisciplinary Optimization*, 66(2):33, 2023.
- [13] D. Lee and S. Rahman. Practical uncertainty quantification analysis involving statistically dependent random variables. *Applied Mathematical Modelling*, 84:324–356, 2020.
- [14] D. Lee and S. Rahman. High-dimensional stochastic design optimization under dependent random variables by a dimensionally decomposed generalized polynomial chaos expansion. *International Journal for Uncertainty Quantification*, 13(4), 2023.
- [15] G. Li and H. Rabitz. D-MORPH regression: Application to modeling with unknown parameters more than observation data. *Journal of Mathematical Chemistry*, 48:1010–1035, 2010.
- [16] G. Li and H. Rabitz. D-MORPH regression for modeling with fewer unknown parameters than observation data. *Journal of Mathematical Chemistry*, 50:1747–1764, 2012.
- [17] S. Li, B. Yang, and F. Qi. Accelerate global sensitivity analysis using artificial neural network algorithm: Case studies for combustion kinetic model. *Combustion and Flame*, 168:53–64, 2016.
- [18] N. J. Linden, B. Kramer, and P. Rangamani. Bayesian parameter estimation for dynamical models in systems biology. *PLOS Computational Biology*, 18(10):e1010651, 2022.
- [19] M. D. Morris. Factorial sampling plans for preliminary computational experiments. *Technometrics*, 33(2):161–174, 1991.
- [20] J. M. Musser and J. E. Carney. Theoretical review of the MFiX fluid and two-fluid models. Technical report, National Energy Technology Laboratory (NETL), Pittsburgh, PA, Morgantown, 2020.
- [21] J. E. Oakley and A. O’Hagan. Probabilistic sensitivity analysis of complex models: a Bayesian approach. *Journal of the Royal Statistical Society: Series B (Statistical Methodology)*, 66(3):751–769, 2004.
- [22] M. M. Opgenoord, D. L. Allaire, and K. E. Willcox. Variance-based sensitivity analysis to support simulation-based design under uncertainty. *Journal of Mechanical Design*, 138(11):111410, 2016.
- [23] E. Qian, B. Peherstorfer, D. O’Malley, V. V. Vesselinov, and K. Willcox. Multifidelity Monte Carlo estimation of variance and sensitivity indices. *SIAM/ASA Journal on Uncertainty Quantification*, 6(2):683–706, 2018.
- [24] S. Rahman. A polynomial dimensional decomposition for stochastic computing. *International Journal for Numerical Methods in Engineering*, 76(13):2091–2116, 2008.
- [25] S. Rahman. Global sensitivity analysis by polynomial dimensional decomposition. *Reliability Engineering & System Safety*, 96(7):825–837, 2011.

- [26] S. Rahman. A surrogate method for density-based global sensitivity analysis. *Reliability Engineering & System Safety*, 155:224–235, 2016.
- [27] D. M. Snider. An incompressible three-dimensional multiphase particle-in-cell model for dense particle flows. *Journal of Computational Physics*, 170(2):523–549, 2001.
- [28] I. M. Sobol. Global sensitivity indices for nonlinear mathematical models and their Monte Carlo estimates. *Mathematics and Computers in Simulation*, 55(1-3):271–280, 2001.
- [29] B. Sudret. Global sensitivity analysis using polynomial chaos expansions. *Reliability Engineering & System Safety*, 93(7):964–979, 2008.
- [30] P. Wang, Z. Lu, and Z. Tang. An application of the Kriging method in global sensitivity analysis with parameter uncertainty. *Applied Mathematical Modelling*, 37(9):6543–6555, 2013.
- [31] J. Xie, W. Zhong, and Y. Shao. Study on the char combustion in a fluidized bed by CFD-DEM simulations: Influences of fuel properties. *Powder Technology*, 394:20–34, 2021.
- [32] J. Xie, W. Zhong, Y. Shao, and K. Li. Coupling of CFD-DEM and reaction model for 3D fluidized beds. *Powder Technology*, 353:72–83, 2019.

Appendix A Sensitivity results for random inputs X_7 – X_{15} in example 2

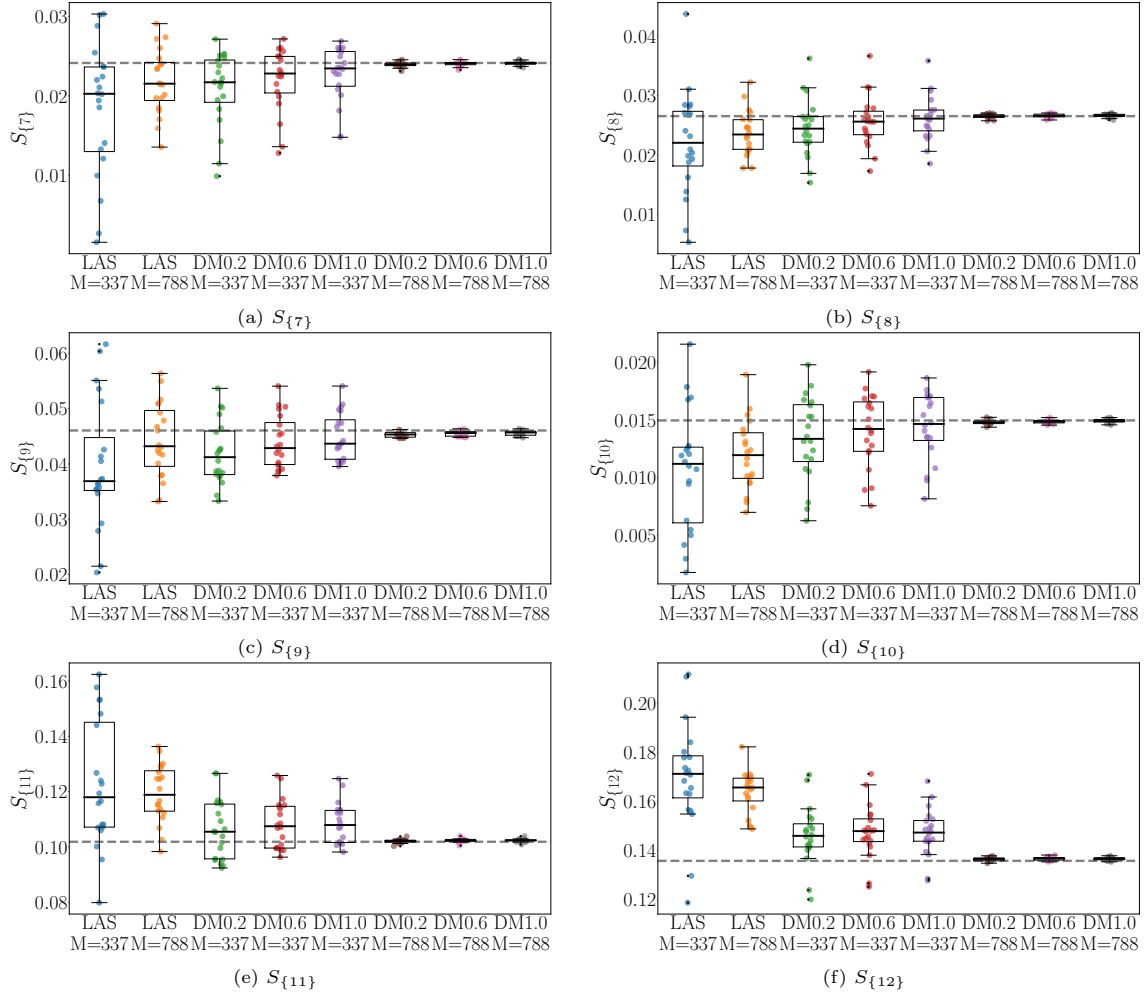


Figure 10: Boxplots of first-order sensitivity indices $S_{\{i\}}$, $i = 7, 8, 9, 10, 11, 12$, of the random output $y(\mathbf{X})$, in (a), (b), (c), (d), (e), (f), respectively, estimated by the bivariate fifth-order PDD using the Lasso (LAS) and Lasso-based D-MOPRH regressions with weight values $\lambda = 0.2, 0.6, 1.0$ (DM0.2, DM0.6, DM1.0). Two underdetermined systems are considered: $M = 337$ and $M = 788$, which correspond to 30% and 70% of the number ($L = 1, 126$) of expansion coefficients. Each regression is repeated 20 times. The exact solution is shown as a gray-dotted line.

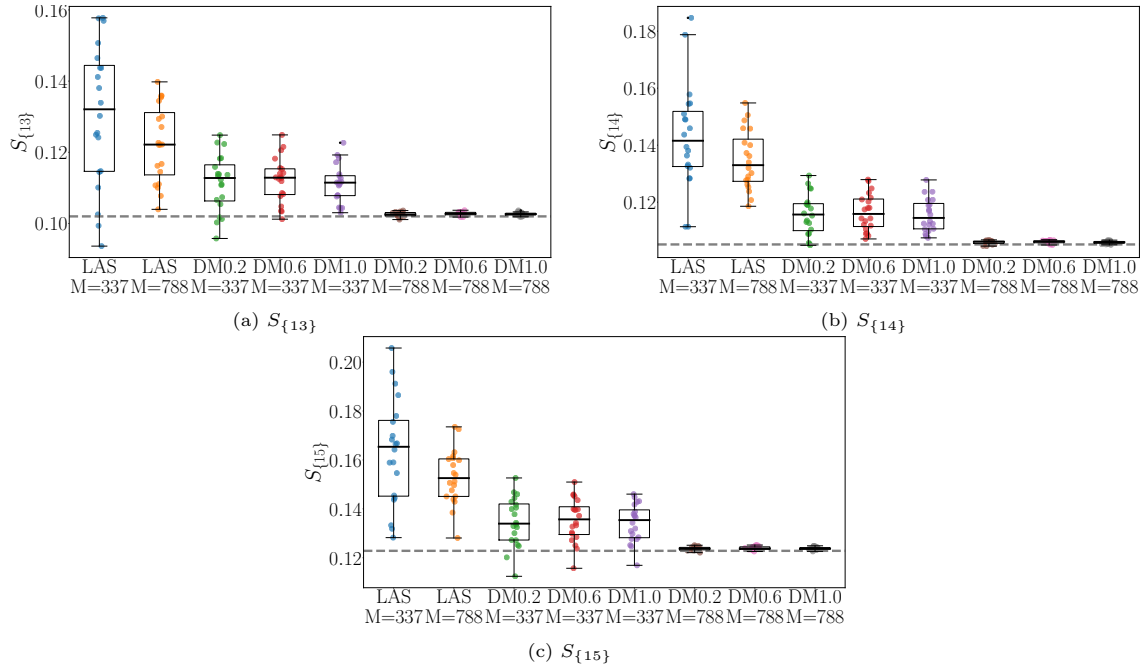


Figure 11: Boxplots of first-order sensitivity indices $S_{\{i\}}$, $i = 13, 14, 15$, of the random output $y(\mathbf{X})$, in (a), (b), (c), respectively, estimated by the bivariate fifth-order PDD using the Lasso (LAS) and Lasso-based D-MOPRH regressions with weight values $\lambda = 0.2, 0.6, 1.0$ (DM0.2, DM0.6, DM1.0). Two underdetermined systems are considered: $M = 337$ and $M = 788$, which correspond to 30% and 70% of the number ($L = 1,126$) of expansion coefficients. Each regression is repeated 20 times. The exact solution is shown as a gray-dotted line.